

An Intermediate-age Alpha-Rich Galactic Population in *K2*

JACK T. WARFIELD,^{1,2,3} JOEL C. ZINN,^{4,1} MARC H. PINSONNEAULT,¹ JENNIFER A. JOHNSON,^{1,5} DENNIS STELLO,^{4,6,7,8}
YVONNE ELSWORTH,^{9,7} RAFAEL A. GARCÍA,^{10,11} THOMAS KALLINGER,¹² SAVITA MATHUR,^{13,14,15} BENOÎT MOSSER,¹⁶
RACHAEL L. BEATON,^{17,*} AND D. A. GARCÍA-HERNÁNDEZ^{14,15}

¹*Department of Astronomy, The Ohio State University, 140 West 18th Avenue, Columbus, OH 43210, USA*

²*Department of Physics, The Ohio State University, 191 West Woodruff Avenue, Columbus, OH 43210, USA*

³*Department of Astronomy, The University of Virginia, 530 McCormick Road, Charlottesville, VA, 22904, USA*

⁴*School of Physics, University of New South Wales, Barker Street, Sydney, NSW 2052, Australia*

⁵*Center for Cosmology and AstroParticle Physics, The Ohio State University Columbus, OH 43210, USA*

⁶*Sydney Institute for Astronomy (SIfA), School of Physics, University of Sydney, NSW 2006, Australia*

⁷*Stellar Astrophysics Centre, Department of Physics and Astronomy, Aarhus University, Ny Munkegade 120, DK-8000 Aarhus C, Denmark*

⁸*Center of Excellence for Astrophysics in Three Dimensions (ASTRO-3D), Australia*

⁹*School of Physics and Astronomy, University of Birmingham, Edgbaston, Birmingham, B15 2TT, UK*

¹⁰*IRFU, CEA, Université Paris-Saclay, F-91191 Gif-sur-Yvette, France*

¹¹*AIM, CEA, CNRS, Université Paris-Saclay, Université Paris Diderot, Sorbonne Paris Cité, F-91191 Gif-sur-Yvette, France*

¹²*Institute of Astrophysics, University of Vienna, Türkenschanzstrasse 17, Vienna 1180, Austria*

¹³*Space Science Institute, 4750 Walnut Street Suite #205, Boulder, CO 80301, USA*

¹⁴*Instituto de Astrofísica de Canarias (IAC), E-38205 La Laguna, Tenerife, Spain*

¹⁵*Departamento de Astrofísica, Universidad de La Laguna (ULL), E-38206 La Laguna, Tenerife, Spain*

¹⁶*LESIA, Observatoire de Paris, PSL Research University, CNRS, Sorbonne Université, Université de Paris Diderot, 92195 Meudon, France*

¹⁷*Department of Astrophysical Sciences, Princeton University, 4 Ivy Lane, Princeton, NJ 08544, USA*

(Received; Revised; Accepted)

Submitted to AJ

Abstract

We explore the relationships between the chemistry, ages, and locations of stars in the Galaxy using asteroseismic data from the *K2* mission and spectroscopic data from the Apache Point Galactic Evolution Experiment survey. Previous studies have used giant stars in the *Kepler* field to map the relationship between the chemical composition and the ages of stars at the solar circle. Consistent with prior work, we find that stars with high $[\alpha/\text{Fe}]$ have distinct, older ages in comparison to stars with low $[\alpha/\text{Fe}]$. We provide age estimates for red giant branch (RGB) stars in the *Kepler* field, which support and build upon previous age estimates by taking into account the effect of α -enrichment on opacity. Including this effect for $[\alpha/\text{Fe}]$ -rich stars results in up to 10% older ages for low-mass stars relative to corrected solar mixture calculations. This is a significant effect that Galactic archaeology studies should take into account. Looking beyond the *Kepler* field, we estimate ages for 735 red giant branch stars from the *K2* mission, mapping age trends as a function of the line of sight. We find that the age distributions for low- and high- $[\alpha/\text{Fe}]$ stars converge with increasing distance from the Galactic plane, in agreement with suggestions from earlier work. We find that *K2* stars with high $[\alpha/\text{Fe}]$ appear to be younger than their counterparts in the *Kepler* field, overlapping more significantly with a similarly aged low- $[\alpha/\text{Fe}]$ population. This observation may suggest that star formation or radial migration proceeds unevenly in the Galaxy.

Keywords: surveys — asteroseismology — stars: abundances — Galaxy: abundances — Galaxy: evolution — Galaxy: stellar content

1. INTRODUCTION

The study of the chemical evolution of the Milky Way has a rich history and a vibrant present. Historically, it has been easier to measure abundances than it has been to measure ages. As a result, most studies have relied on abundance data alone—for example, very low absolute iron abundance, or characteristic heavy element abundance patterns relative to iron—as indicators of membership in old populations. However, we can now measure ages for large samples of evolved stars using stellar pulsation—or asteroseismic—data from large time domain surveys, and we have an unprecedented wealth of abundance data from massive spectroscopic surveys. These new tools allow us to trace out the enrichment history of the Milky Way in a far more detailed fashion than was possible even a few years ago. In this paper we focus on ages for evolved red giants with enhanced abundances of α -capture elements relative to iron compared to the Sun, which we will refer to as α -rich stars.

The existence of α -rich stars has been known for over half a century (Aller & Greenstein 1960; Wallerstein 1962). The α -capture elements—such as O, Mg, Si, S, Ca, and Ti—are primarily produced in core-collapse supernovae of massive, short-lived stars (SNe II). Fe-peak elements, by contrast, can also be injected into interstellar medium by the explosive destruction of a white dwarf (a Type Ia supernova, SNe Ia). The latter process requires a longer-lived progenitor. Therefore, in very old populations, such as the Galactic halo, stars are thought to be α -rich because they formed before SNe Ia occurred in significant numbers (Tinsley 1979).

In a simple chemical evolution model, the $[\alpha/\text{Fe}]$ ratio of the gas would decline as the number of SNe Ia contributing Fe-peak elements increases, before reaching an equilibrium ratio (e.g., Weinberg et al. 2017). This is not what is observed in the solar neighborhood (Prochaska et al. 2000; Bensby et al. 2003). Rather than a single sequence from high- α to low- α , stars with $-1 < [\text{Fe}/\text{H}] < 0$ can have a range of $[\alpha/\text{Fe}]$ values. The origin of this bi-modal α sequence of stars in the Galaxy is still a puzzle. Bensby et al. (2003) showed that there are distinct trends in $[\alpha/\text{Fe}]$ vs. $[\text{Fe}/\text{H}]$ space for the geometrically defined thin and thick discs (Gilmore & Reid 1983). Hayden et al. (2015) investigated how these

trends behave as a function of Galactic radius (R) and height above the Galactic plane (Z) using $\sim 70,000$ red giants from the Sloan Digital Sky Survey (SDSS) Apache Point Galactic Evolution Experiment (APOGEE) Data Release (DR) 12. These authors found the high- α part of this sequence strongly present only at $|Z| > 0.5$ kpc and $R < 11$ kpc.

Because of the origins of the α elements, the α -rich and α -poor populations must be somehow tied to the history of SNe II and Ia. However, all of the observed patterns—for instance, the spread in $[\alpha/\text{Fe}]$ at a given $[\text{Fe}/\text{H}]$ —cannot be explained by the SNe history alone. Therefore, other, more complex mechanisms must also contribute to the formation of the observed chemical and age patterns. Some proposed mechanisms capable of reproducing the observed sequences are the radial migration of stars in the Galaxy (see, e.g., Sellwood & Binney 2002; Schönrich & Binney 2009; Nidever et al. 2014; Weinberg et al. 2017; Sharma et al. 2020); two separate star formation episodes driven by pristine gas infall into the Galaxy (e.g. Chiappini et al. 1997; Spitoni et al. 2019; Lian et al. 2020); and stars forming throughout the Galaxy in clumpy bursts (e.g. Clarke et al. 2019). Though all are able to roughly recreate the observed chemical pattern, each of these mechanisms are responsible for different predictions concerning the relative ages of the α -rich and α -poor populations and how homogeneous these results will be across the Galaxy. Therefore, finding ages for stars as functions of their chemical abundances and locations in the Galaxy is an important step in uncovering the mechanisms that are responsible for the Galaxy’s formation.

Finding ages for large numbers of field red giants up to several kpc away from the Sun is now possible through asteroseismology. Near-surface turbulent convective motions in cool stars generate sound waves, and for distinct resonant frequencies of the stellar interior, standing waves can be induced, forming a frequency pattern of overtone modes of different spherical degrees. The frequency spacings between the radial modes ($\Delta\nu$) is related to the mean density (Ulrich 1986; Kjeldsen & Bedding 1995). The frequency of maximum acoustic power (ν_{max}) is related to the acoustic cut-off frequency, and therefore the density scale height and the surface gravity (Brown et al. 1991; Kjeldsen & Bedding 1995; Chaplin et al. 2008). It is therefore possible to solve for mass and radius through scaling relations if $\Delta\nu$, ν_{max} , and T_{eff} are known. Pinsonneault et al. (2014, 2018)

* Hubble Fellow
Carnegie-Princeton Fellow

produced catalogs of values for ν_{\max} , $\Delta\nu$, asteroseismic masses & radii, chemical abundance estimates, and age estimates for targets in the fields observed photometrically by NASA’s *Kepler* mission and spectroscopically by APOGEE.

Ages for the α -rich and α -poor populations in the Pinsonneault et al. (2014) data set—including sample selection effect corrections—were calculated by Silva Aguirre et al. (2018) (hereafter SA18). These ages were found using different asteroseismic corrections than used for the ages published by Pinsonneault et al. (2018). Partially motivated by finding chemical signatures that can be used as tracers of the thin and thick disks, SA18 used a combination of photometric, spectroscopic, and asteroseismic parameters to estimate the ages of 1590 red giant branch and red clump stars located within the *Kepler* field. They found that the population of giants with low $[\alpha/\text{Fe}]$ has a distribution peaked at ~ 2 Gyr and slopes gradually down to older ages, whereas the population with high $[\alpha/\text{Fe}]$ peaks strongly at ~ 11 Gyr. The ages of these populations were found to have limited overlap, with a transition at ~ 8 Gyr, results which coincide with the observed ages in the solar neighborhood from Fuhrmann (1998, 2011). These results have been corroborated and expanded on by Miglio et al. (2020), who found ages for 5400 giants in the *Kepler* field. SA18 also found a surprising, small population of very young, α -rich stars which, though possibly high-mass stars with genuinely young ages, could also indicate an unexpectedly large population of merger products—stars that have gained mass from a companion and therefore look younger than they actually are (Martig et al. 2015; Chiappini et al. 2015). Investigations of populations along other lines of sight have the potential to clarify the origin of this unusual cohort. The relationship shown by SA18 between age and α -enrichment agrees very well with what might be expected if only considering the contribution of historic SNe rates to the interstellar medium. However, the sample of stars available from Pinsonneault et al. (2014, 2018), and SA18’s sub-sample, represent a population of stars very local to the Sun, only extending out to a distance of about 2 kpc. Therefore, whether these results are true for the α -rich and α -poor populations outside of the solar circle is still relatively uncertain.

In an effort to characterize the age distributions with asteroseismology outside of the solar vicinity, Anders et al. (2017) combined asteroseismology from two of the *CoRoT* fields with APOGEE DR12 to get masses, radii, and ages using the Bayesian parameter estimation code PARAM (da Silva et al. 2006; Rodrigues et al. 2014). These fields, lying very close to the Galactic plane, pro-

vide a valuable sampling of the Milky Way’s chemical history at a range of Galactic radii.

Building on work from *Kepler* and *CoRoT*, our paper takes advantage of the multiple Galactic sight-lines that the *K2* mission (Howell et al. 2014) affords to better understand the age distributions of stars outside of the immediate solar neighborhood. Following the failure of the *Kepler* satellite’s pointing, a new observing strategy was adopted to use the solar wind for partial stabilization. The re-purposed *Kepler* mission, dubbed *K2*, could no longer focus on the original *Kepler* field. However, by virtue of its ecliptic orientation, it could now observe fields of view along the ecliptic for ~ 80 days at a time (Howell et al. 2014). *K2* therefore offers an expanded view of the Galaxy compared to the *Kepler* prime mission, and thanks to a dedicated program to target red giants, the *K2* Galactic Archaeology Program (K2 GAP; Stello et al. 2015), has yielded asteroseismic data beyond the solar vicinity (Stello et al. 2017). As proof of the usefulness of *K2* for Galactic archaeology, ages were found by Rendle et al. (2019) for stars in *K2* campaigns 3 and 6. This includes a confirmation of the existence of young, α -rich stars that otherwise are consistent with sharing the kinematic properties of old α -rich stars.

In this paper, we look to further investigate the relationship between α abundance and age by combining asteroseismic data obtained from observations of red giants observed by *K2* with spectroscopic data from APOGEE DR16. Giants in the *K2* fields, many of which were targeted at greater distances compared to the *Kepler* giants, offer the opportunity to discover properties of α -rich and α -poor populations well beyond the solar circle. §2 describes how we selected the sample. In §3 we describe how we were able to obtain accurate age estimates for the sample of red giants. In §4 we discuss the ages that we found for the α -rich and α -poor populations in the *K2* fields and touch on some possible implications for the Galactic formation mechanisms mentioned above.

2. DATA SELECTION

The spectroscopic data for this work is from the 16th data release of the APOGEE survey (Majewski et al. 2017; Ahumada et al. 2020). This survey has been collecting high resolution IR spectra for hundreds of thousand of stars throughout the Milky Way. Access is provided to both the raw spectra and derived estimates for stellar parameters such as effective temperature (T_{eff}), surface gravity (g), and chemical abundances via an automated pipeline. This includes estimates for metal-

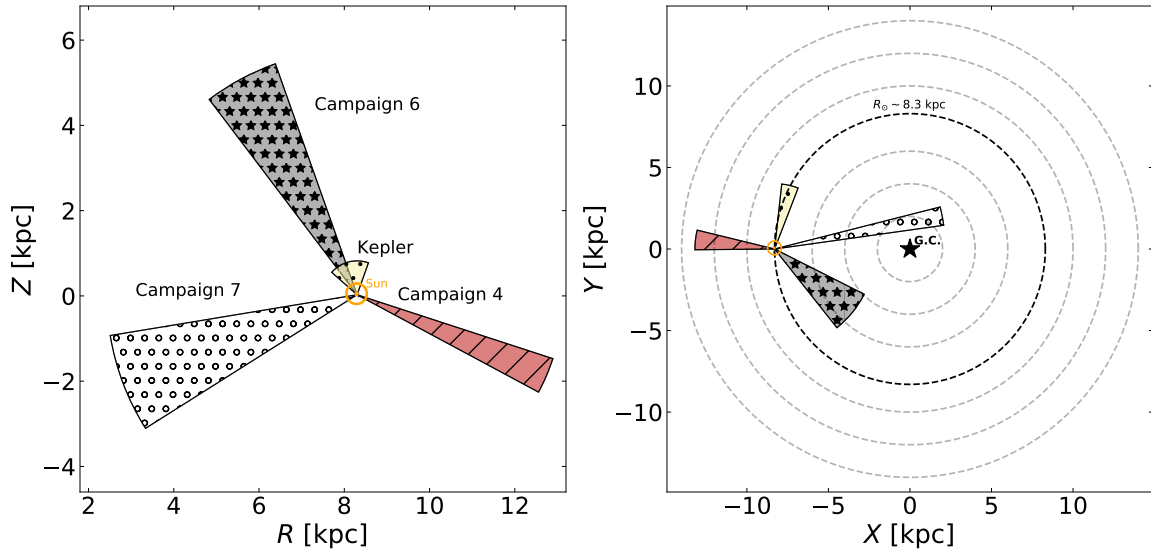


Figure 1. Schematics showing the approximate lines of sight for *K2* campaigns 4, 6, and 7. The plot on the left shows the fields in the Galactocentric coordinates Z (height above or below the Galactic plane) and R (radial distance from the Galactic center). The plot on the right shows these fields in the Galactocentric X and Y coordinates. The Sun is approximated to be at $R = 8.3$ kpc, $Z = 0.027$ kpc, $X = -8.3$ kpc, and $Y = 0$ kpc. Our sample contains 160 stars in C4, 411 stars in C6, and 233 stars in C7.

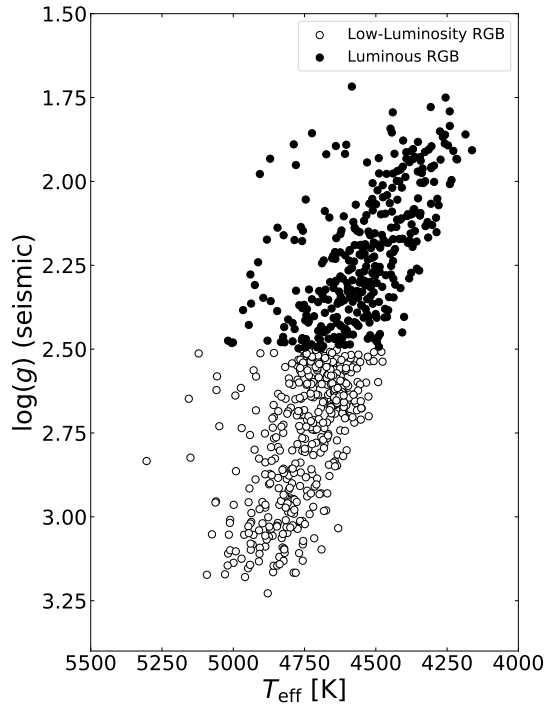


Figure 2. Kiel diagram for our sample of stars using effective temperatures from APOGEE and surface gravities calculated from the *K2* GAP DR2 asteroseismic parameters. Low-luminosity giants are defined here as giants with $\log(g) > 2.5$.

licity ($[\text{Fe}/\text{H}]$) and α -enrichment ($[\alpha/\text{M}]^1$). The spectroscopic data in APOGEE DR16 was collected with the 2.5-meter Sloan Foundation Telescope (Gunn et al. 2006) at the Apache Point Observatory in New Mexico and the 2.5-meter du Pont Telescope (Bowen & Vaughan 1973) at Las Campanas Observatory in Chile as a part of SDSS-IV (Blanton et al. 2017). APOGEE uses twin $R \sim 22,500$ H-band spectrographs (Wilson et al. 2019). APOGEE deliberately targeted red giants in the *Kepler* and *K2* fields to provide spectroscopic data for seismically detected stars. The selection of red giants in the *Kepler* field is presented in Zasowski et al. (2013, 2017), while the APOGEE program in the *K2* fields is presented in Zasowski et al. (2017) and Beaton et al. (in preparation). Briefly, the *K2* program’s stars were selected in a priority scheme as follows: (1) known planet hosts, (2) confirmed oscillators, (3) red giant targets in the GAP and not observed with HERMES, (4) red giants targeted in the GAP and observed with HERMES, (5) M-dwarf candidates, and (6) filler giants following the APOGEE-2 main red star sample (Zasowski et al. 2017). Field centers were chosen to maximize the total priority and targets were selected in each field following the typical APOGEE fashion (Zasowski et al. 2013).

The general scheme for extraction of the spectra, wavelength calibration, latfielding, and radial velocity

¹ $[\alpha/\text{Fe}]$ and $[\alpha/\text{M}]$ are conceptually equivalent, with the $[\alpha/\text{M}]$ parameter used by APOGEE measuring the ratio of α elements to the overall metallicity rather than just to iron.

measurements is described in [Nidever et al. \(2015\)](#), with updates in [Holtzman et al. \(2018\)](#) and [Jönsson et al. \(2020\)](#). Stellar parameters are obtained by processing the spectra through the APOGEE Stellar Parameters and Chemical Abundances Pipeline (ASPCAP) which infers these values by fitting the spectra to a grid of synthetic spectra (for a description of the pipeline, see [García Pérez et al. 2016](#)). [Jönsson et al. \(2020\)](#) describes the updates to the pipeline for DR16, including the use of MARCS atmospheres for all stars with $T_{\text{eff}} < 8000$ K. [Smith et al. \(in preparation\)](#) describes the new line list used for construction of synthetic spectra in DR16.

Asteroseismic data for this work comes from the 2nd data release of *K2* GAP ([Zinn et al. 2020](#)). Over the mission lifespan, *K2* made observations along 19 different lines-of-sight across the Galaxy which are referred to as campaigns 0-18. *K2* GAP provides the analysis of asteroseismic targets in these fields. Because of the shorter time spent observing each of these fields versus the *Kepler* field (~ 80 days versus 4 years), the associated uncertainties with the asteroseismic parameters are significantly larger. However, the data from *K2* offers a much more diverse positional sampling of stars in the Galaxy. The full *K2* GAP project covers *K2* campaigns 1-18 over a series of three data releases. Data Release 1 ([Stello et al. 2017](#)) provided analysis for ~ 1200 stars in *K2* campaign 1 and worked as a proof of concept for the project. Data Release 2, used in this work, provides analysis of ~ 4500 stars in *K2* campaigns 4, 6, and 7. These three campaigns were chosen as they probe three lines of sight that are both distinct from each other and from the *Kepler* field (Figure 1). Data Release 3 will provide the results for the remaining *K2* campaigns.

Following methods developed for *Kepler* ([Pinsonneault et al. 2018](#)), *K2* GAP DR2 improves on *K2* GAP DR1 by providing asteroseismic data that have been averaged across results from up to six independent pipelines. These pipelines are A2Z+ (based on [Mathur et al. 2010](#)), BHM ([Elsworth et al. 2020](#); [Hekker et al. 2010](#)), CAN ([Kallinger et al. 2016](#)), COR ([Mosser & Apourchaux 2009](#)), SYD ([Huber et al. 2009](#)), and BAM ([Zinn et al. 2019b](#)). In this paper, we only consider giants in this catalog for which at least two of these pipelines returned values for both ν_{max} and $\Delta\nu$, and take the mean of these results. We include these mean values along with all of the associated pipeline values in our catalog.

To investigate trends in the age-abundance relationship with Galactic position, we adopted Bayesian distance estimates based on *Gaia* Data Release 2 ([Gaia Collaboration et al. 2016, 2018](#)) parallaxes from [Bailer-Jones \(2015\)](#). Each star’s height above the Galactic

plane (Z), radial distance from the center of the Galaxy (R), and Galactocentric X and Y coordinates were computed using [Astropy²](#) ([Astropy Collaboration et al. 2013](#); [Price-Whelan et al. 2018](#)).

We have extensive asteroseismic data sets for both shell H-burning red giant branch (RGB) stars and core He-burning red clump (RC) stars. We restrict ourselves to RGB stars because the mapping between mass and age for RC stars is complicated by the known existence of mass-loss between the RGB and RC phases, so that the present-day RC asteroseismic mass is systematically biased compared to its birth mass (e.g., [Casagrande et al. 2016](#)).

The state-of-the-art for RGB vs. RC classifications is to determine a star’s evolutionary state through asteroseismology (e.g., [Bedding et al. 2011](#)). However, this method requires very long time domain data. Though these classifications are difficult to do with the short *K2* time series, they have been successfully made using the *Kepler* data by [Elsworth et al. \(2019\)](#).

To distinguish between RGB and RC stars in *K2*, we used a spectroscopic evolutionary state classification similar to that of [Bovy et al. \(2014\)](#). A temperature-, surface gravity-, and abundance-dependent cut to separate RGB and RC stars was found using the evolutionary states from [Elsworth et al. \(2019\)](#). First, we fit for α , β , and γ that define a “reference” temperature given by

$$T_{\text{ref}} = \alpha + \beta [\text{Fe}/\text{H}]_{\text{RAW}} + \gamma (\log(g)_{\text{SPEC}} - 2.5) \quad (1)$$

through a non-linear least squares fit for stars classified as RGB according to APOKASC-2 asteroseismology. $[\text{Fe}/\text{H}]_{\text{RAW}}$ and $\log(g)_{\text{SPEC}}$ are the uncorrected values for metallicity and surface gravity, respectively, given in the APOGEE DR16 catalogue. The fitting results were found to have approximate values of $\alpha = 4383.148$ K, $\beta = -235.136$ K/dex, and $\gamma = 532.659$ K/dex. A line was then fit through the approximate ridgeline in $[\text{C}/\text{N}]_{\text{RAW}}$ vs. $T_{\text{eff}}^{\text{SPEC}} - T_{\text{ref}}$ space for which 98% of stars to the right of the line were classified as RGB. This ensures that the contamination from RC stars in our spectroscopic classifications is negligible. The finalized classification criteria in Table 1 were then used to pick out the stars in our *K2* sample that are most likely to be on the RGB. Hereafter in this work, all references to “giants” refer specifically to RGB stars unless otherwise stated.

From the parameters provided by *K2* GAP and APOGEE, we were able to calculate values for asteroseismic surface gravity ($\log(g)_{\text{seis}}$), for mass, and for

² <https://www.astropy.org>

Table 1. Grid for if a star is classified as a red giant for different ranges of $\log(g)_{\text{SPEC}}$ and $[\text{C}/\text{N}]_{\text{RAW}}$. Stars are classified as red giants if the statement for the given range of conditions is true for that star. $\Delta T = T_{\text{eff}}^{\text{SPEC}} - T_{\text{ref}}$.

	$3.5 > \log(g)_{\text{SPEC}} > 2.38$	$\log(g)_{\text{SPEC}} < 2.38$
$[\text{C}/\text{N}]_{\text{RAW}} > -0.2969$	$[\text{C}/\text{N}]_{\text{RAW}} < 0.0209 - 0.5352[\text{Fe}/\text{H}]_{\text{RAW}} - 0.0029\Delta T$	True
$[\text{C}/\text{N}]_{\text{RAW}} < -0.2969$	$150 > 182.662[\text{Fe}/\text{H}]_{\text{RAW}} + \Delta T$	True

radius. $\log(g)_{\text{seis}}$ was calculated using ν_{max} and T_{eff} in the scaling relation (Brown et al. 1991; Kjeldsen & Bedding 1995):

$$\left(\frac{\nu_{\text{max}}}{\nu_{\text{max},\odot}}\right) \approx \left(\frac{g}{g_{\odot}}\right) \left(\frac{T_{\text{eff}}}{T_{\text{eff},\odot}}\right)^{-1/2}, \quad (2)$$

with solar reference values of $\nu_{\text{max},\odot} = 3076 \mu\text{Hz}$, $T_{\text{eff},\odot} = 5772 \text{K}$, and $g_{\odot} = 27400 \text{cm/s}^2$.³ Values for mass and radius can be found by combining Equation 2 with the scaling relation for $\Delta\nu$ (Ulrich 1986; Kjeldsen & Bedding 1995),

$$\Delta\nu \propto M^{1/2} R^{-3/2}. \quad (3)$$

Doing this gives that

$$\left(\frac{M}{M_{\odot}}\right) \approx \left(\frac{\nu_{\text{max}}}{f_{\nu_{\text{max}}}\nu_{\text{max},\odot}}\right)^3 \left(\frac{T_{\text{eff}}}{T_{\text{eff},\odot}}\right)^{3/2} \left(\frac{\Delta\nu}{f_{\Delta\nu}\Delta\nu_{\odot}}\right)^{-4} \quad (4)$$

and

$$\left(\frac{R}{R_{\odot}}\right) \approx \left(\frac{\nu_{\text{max}}}{f_{\nu_{\text{max}}}\nu_{\text{max},\odot}}\right) \left(\frac{T_{\text{eff}}}{T_{\text{eff},\odot}}\right)^{1/2} \left(\frac{\Delta\nu}{f_{\Delta\nu}\Delta\nu_{\odot}}\right)^{-2}. \quad (5)$$

We adopt $\Delta\nu_{\odot} = 135.146 \mu\text{Hz}$. We also compute theoretically-motivated corrections to the observed $\Delta\nu$ values, $f_{\Delta\nu}$, according to Sharma et al. (2016). There is increasing empirical evidence that these and similar corrections from the literature (e.g., White et al. 2011; Guggenberger et al. 2017) result in better agreement with independent estimates of stellar parameters (e.g., Huber et al. 2017). Evaluating $f_{\Delta\nu}$ requires mass, radius, temperature, evolutionary state, and metallicity. The bulk metallicities are adjusted for this purpose to account for non-solar alpha abundances according to the Salaris et al. (1993) prescription: $[\text{Fe}/\text{H}]' = [\text{Fe}/\text{H}] + \log_{10}(0.638 \times 10^{[\alpha/\text{M}]} + 0.362)$. We assume that there are no corrections needed to the observed ν_{max} values (i.e., $f_{\nu_{\text{max}}} = 1$), pending further empirical constraints and theoretical understanding of the ν_{max} scaling relation (see discussion in, e.g., Pinsonneault et al. 2018).

The sample was then further limited to stars with $[\alpha/\text{M}]$ values between 0.0 and 0.4 dex, $[\text{Fe}/\text{H}]$ values between -2.0 and 0.6 dex, and masses between 0.6 and 2.6

M_{\odot} in order to ensure meaningful parameter values that fit within the parameter space defined by the tracks that we used for estimating ages (§3). It should be noted that it is still unclear how well the asteroseismic scaling relations work for low-metallicity stars with $[\text{Fe}/\text{H}] < -1$ (e.g., Epstein et al. 2014; Valentini et al. 2019), however, the inclusion of these few objects in our sample does not have a noticeable impact on our results for the bulk populations. As a final quality check, we consider low- and high- luminosity RGB stars separately in §4. High-luminosity giants appear to suffer from measurement systematics (Mosser et al. 2013; Pinsonneault et al. 2018; Zinn et al. 2019a) and so, out of an abundance of caution, we employ a conservative surface gravity cut to separate our sample: stars with $\log(g)_{\text{seis}} < 2.5$ are classified as luminous giants and stars with $\log(g)_{\text{seis}} > 2.5$ are classified as low-luminosity giants (Figure 2).

Lastly, the sample was divided into the categories of α -rich and α -poor by approximately drawing a line through the ridge-line between the two populations, as seen in Figure 3.

3. AGE DETERMINATION

Obtaining reliable ages for RGB stars is primarily dependent on having accurate estimates for stellar mass and secondarily on harmoniously-calibrated values for chemical compositions. Because the lifetime in the RGB phase is short, the surface gravity has only a minor impact on the derived age, especially on the upper RGB. Because of mechanical challenges in incorporating the age dependence tied to surface gravity, which is multi-valued for the RGB, we simply bracket our sample into two surface gravity bins and take the age range within these bins as a (very small) additional source of uncertainty.

At fixed surface gravity and composition, age is strongly sensitive to effective temperature. In grid modeling, the derived age combines this information with asteroseismic properties; for an example see SA18. However, there are large random and systematic uncertainties in this age estimate due to effective temperature offsets. On the giant branch locus, an error budget of 50 K in temperature would produce a random age uncertainty of $\sim 70\%$. A mismatch between the true locus of the seismic data and stellar models can also produce very large zero-point offsets and composition-dependent

³ This value agrees to within 0.0003 dex with the recent standard solar values adopted in Mamajek et al. 2015.

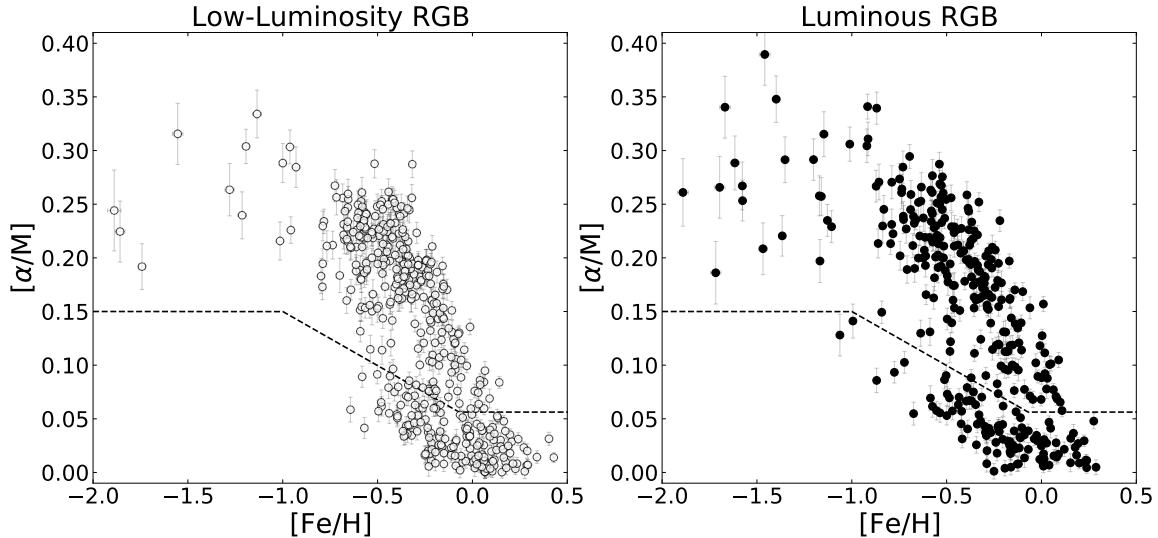


Figure 3. $[\alpha/M]$ vs. $[\text{Fe}/\text{H}]$ for the low-luminosity and luminous giants in our sample. Our sample is further split into the categories of α -rich and α -poor, which is defined by the dashed line in the plots. This division was defined by-eye based on the ridge-line between the groups of points in the data. This cut is similar to that made by e.g. [Silva Aguirre et al. \(2018\)](#) and [Weinberg et al. \(2019\)](#). This line is defined as $[\alpha/M] = 0.15$ for $[\text{Fe}/\text{H}] < -1.0$, $[\alpha/M] = 0.056$ for $[\text{Fe}/\text{H}] > -0.07$, and $[\alpha/M] = -0.1 \cdot [\text{Fe}/\text{H}] + 0.049$ for $-1.0 \leq [\text{Fe}/\text{H}] \leq -0.07$.

systematic shifts ([Tayar et al. 2017](#)). We therefore adopt the methodology of [Pinsonneault et al. \(2018\)](#), and do not directly incorporate classical age constraints from HR diagram position. We note that this choice also makes the ages more replicable, and that others can use different choices of stellar models with these data to infer ages with a grid modeling approach if they so choose.

We used stellar evolutionary tracks, generated with the Yale Rotating Evolution Code, from [Pinsonneault et al. \(1989\)](#) with updates from [van Saders & Pinsonneault \(2012\)](#). From these tracks we created three sets of grids for $\log(g)$ of 3.30, 2.50, and 1.74, with columns for $\log(\text{Mass})$, $[\text{Fe}/\text{H}]$, $[\alpha/\text{Fe}]$, and $\log(\text{age})$. These values for $\log(g)$ were chosen to approximately bracket the low-luminosity giant branch (3.30 and 2.50) and the upper giant branch (2.50 and 1.74). We made these grids regular along the $\log(\text{Mass})$, $[\text{Fe}/\text{H}]$, and $[\alpha/\text{Fe}]$ axes by linearly interpolating to ages at locations where there were gaps in the tracks. Given a star’s values and associated uncertainties for each of these parameters, a Monte Carlo method was used to calculate 500 age estimates for each star through 4-point Lagrange interpolation within the grid. The reported results for a given star is the median of these values along with a lower and an upper $1\text{-}\sigma$ uncertainty reflecting the 16th and 84th percentiles of the Monte Carlo results, respectively.

Figure 4 shows a comparison between the ages calculated for 2407 RGB stars in the *Kepler* field using this method and the ages reported for the same giants in the APOKASC-2 catalog ([Pinsonneault et al. 2018](#)).

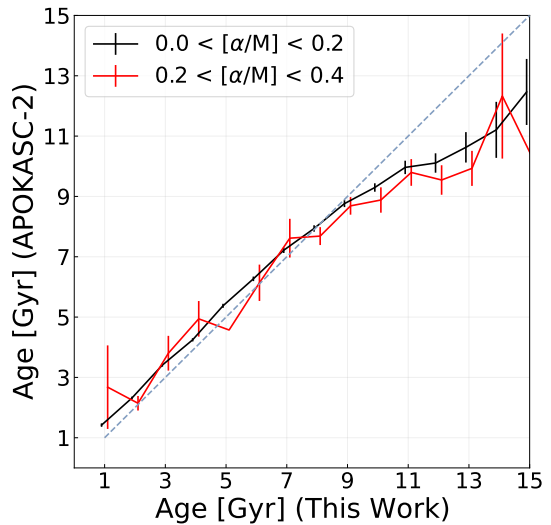


Figure 4. A comparison of the ages reported in the APOKASC-2 catalog vs. the ages calculated for this work for 2407 RGB stars from [Pinsonneault et al. \(2018\)](#). Error bars represent the standard deviation of the mean for bins that are 1 Gyr wide on the x -axis.

There are a few main systematic effects, aside from differences in technique, that lead to the slight disagreement in the ages and the age zero-point. First, though [Pinsonneault et al. \(2018\)](#) used a similar method to estimate the ages of these stars, the stellar tracks and isochrones used did not take α enhancement into account when generated. Rather, the lookup metallicity was corrected by adjusting $[\text{Fe}/\text{H}]$ by $+0.625 [\alpha/M]$. At

a fixed $[\text{Fe}/\text{H}]$, an increase in $[\alpha/\text{M}]$ corresponds to an increase in a star’s opacity. Increasing a star’s opacity means also increasing its radius, therefore lowering the star’s core temperature and extending the amount of time that it takes to burn through core hydrogen on the main sequence. Therefore, not considering $[\alpha/\text{M}]$ in stellar models has the effect of underestimating the ages of stars with $[\alpha/\text{M}] > 0$, with the biggest effect being for the ages of low-mass stars. The correction on metallicity used by Pinsonneault et al. (2018) is not able to fully account for this effect. On average, this affects the ages of stars younger than about 8 Gyr by approximately +1% and above 8 Gyr by +8%. The second systematic is that, in order to make the ages in the *Kepler* field more concordant with those from the *K2* fields, we recalculated $f_{\Delta\nu}$ for this sample in the same manner that it was calculated for *K2* GAP. This adjustment leads to changes in mass by an average of about +2% to +3%, which corresponds to changes of -6% to -9% in age. In order to make masses agree with those from open clusters, Pinsonneault et al. (2018) applied a uniform shift in $f_{\nu_{\text{max}}}$ (and therefore the sample’s asteroseismic masses). Correcting the zero-point offset from our reformulation of values for $f_{\Delta\nu}$ so that the masses are on the same open cluster scale, therefore, required us to scale masses for the *Kepler* sample down by a factor of 1.018, which translates to scaling ages up by a factor of about $1.018^3 = 1.055$ (or about 6%). In addition to these effects, there are also going to be changes associated with the difference between the abundance estimates in APOGEE DR14 (which was used for the ages by Pinsonneault et al. 2018) and APOGEE DR16 (changes between these data releases are discussed in Jönsson et al. 2020).

Another check we can perform on the data is to see if our age distributions for *Kepler* stars reproduce the features seen by SA18. The ages published by SA18 are computed using the Bayesian stellar parameter estimation package BASTA (Silva Aguirre et al. 2015, 2017). The *Kepler* age distribution globally reproduces the features of that from SA18, including the small young, α -rich population. This indicates that adopting a grid modeling approach does not induce a large change in derived ages. We also note that our *Kepler* age distribution is consistent with recent estimates of the thick disk age using detailed asteroseismic modeling of *Kepler* data (Montalbán et al. 2020).

4. RESULTS AND DISCUSSION

The panels in Figure 5 show the age results from both the *Kepler* and *K2* fields. Results are shown for both the full samples and for the low-luminosity giants

in each field. Figure 6 shows these same results for each *K2* campaign individually. Gaussian kernel density functions were drawn over each distribution using the `kdeplot` function from the `seaborn`⁴ Python package (Waskom et al. 2017). We can see that, though the inclusion of the luminous giants does not have a significant impact on the locations of the peaks for the underlying kernel density estimates they do contribute a noticeable degree of scatter to the results..

Table 2 summarizes these results for the α -rich giants in each field. Our full *K2* data sample, including age estimates for individual stars, are provided in Table 3. Table 4 contains our ages for stars in the *Kepler* field.

Comparing our results for these *K2* fields with the results from the *Kepler* field brings to light two interesting differences. First, though the median age of the α -rich population is strongly peaked at a single age in both of these samples, the populations in the *K2* fields are found to be at an age about 2 Gyr younger than what was found in the *Kepler* field. Secondly, there seems to be much less of a difference between the ages of the α -rich and α -poor populations in the *K2* field.

Of course, it is still possible that there are systematics at play partially driving these discrepancies. The *K2* asteroseismic parameters used in this work yield radii that may be up to $\sim 2\%$ larger than radii computed based on *Gaia* DR2 parallaxes (Zinn et al. 2020). Assuming this offset is due to slightly different ν_{max} scale compared to APOKASC-2, this implies that the *K2* masses may be too large by $\sim 5\%$, which would allow for the *K2* ages to be $\sim 15\%$ younger than the *Kepler* ages. In this sense, the age gap we find between *K2* and *Kepler* may be related to the fundamental scale of the *K2* asteroseismic data. At this time, we are limited in our ability to calibrate the *K2* asteroseismic scale with *Gaia* data due to the *Gaia* DR2 parallax zero-point varying across the sky. The next data release of *Gaia* data should be less affected by the zero-point, and will be very useful in solidifying the *K2* asteroseismic scale (see also Khan et al. 2019).

There is, however, some reason to believe that an intermediately aged α -rich population could be physical: Lian et al. (2020) discuss a population of young, α -rich stars in the outer disk, suggesting that there should have also been mechanisms in place to make the intermediate age populations observed in *K2*. In addition, the result from Anders et al. (2017) of a young α -rich population with similar ages to the corresponding α -poor population in the *CoRoT* fields seems to also indicate

⁴ <https://seaborn.pydata.org>

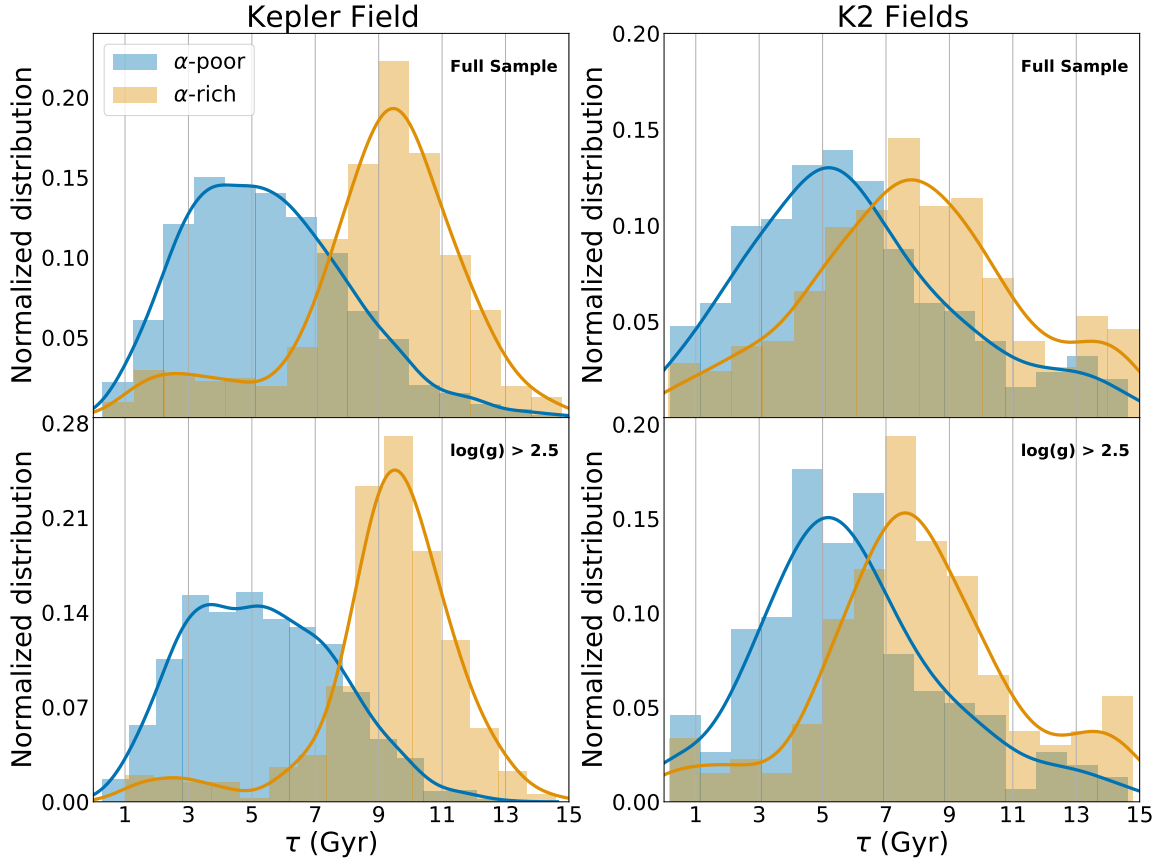


Figure 5. Distributions of the age estimates for the Kepler field (left) and *K2* fields (right) for both the α -poor (blue) and α -rich (orange) populations. The top row shows the distributions for the full sample for the respective fields and the bottom row shows the distributions for the low-luminosity sample ($\log(g)_{\text{seis}} > 2.5$). In the *Kepler* field, there are 691 (389) α -rich and 1714 (1228) α -poor stars in the full (low-luminosity) sample. In the *K2* fields, there are 534 (291) α -rich and 270 (160) α -poor stars in the full (low-luminosity) sample.

Table 2. This table gives information for the kernel density estimation (kde) and the underlying data for the age-distributions of the low-luminosity α -rich populations in each field (shown in Figures 5 and 6). The value for the α -rich age width is calculated as $\text{FWHM}/2.355$, where FWHM is the full width at half maximum around the peak in the kde. The mean error is the average error in the age estimate for only the α -rich stars in the indicated field. The possible systematic uncertainties come from the interpolation error (-1%) and from the systematic uncertainty due to the *K2* ν_{max} scale (+15%).

Field	α -rich Peak Age (Gyr)	α -rich Peak Age Width (Gyr)	Average Age Uncertainty (Gyr)	Possible Sys. Uncertainties (%)
Kepler	9.53	1.40	1.46	-1
K2 C4	8.08	3.83	2.92	+14
K2 C6	7.62	2.16	2.23	+14
K2 C7	7.24	2.63	2.40	+14
all K2	7.61	2.17	2.32	+14

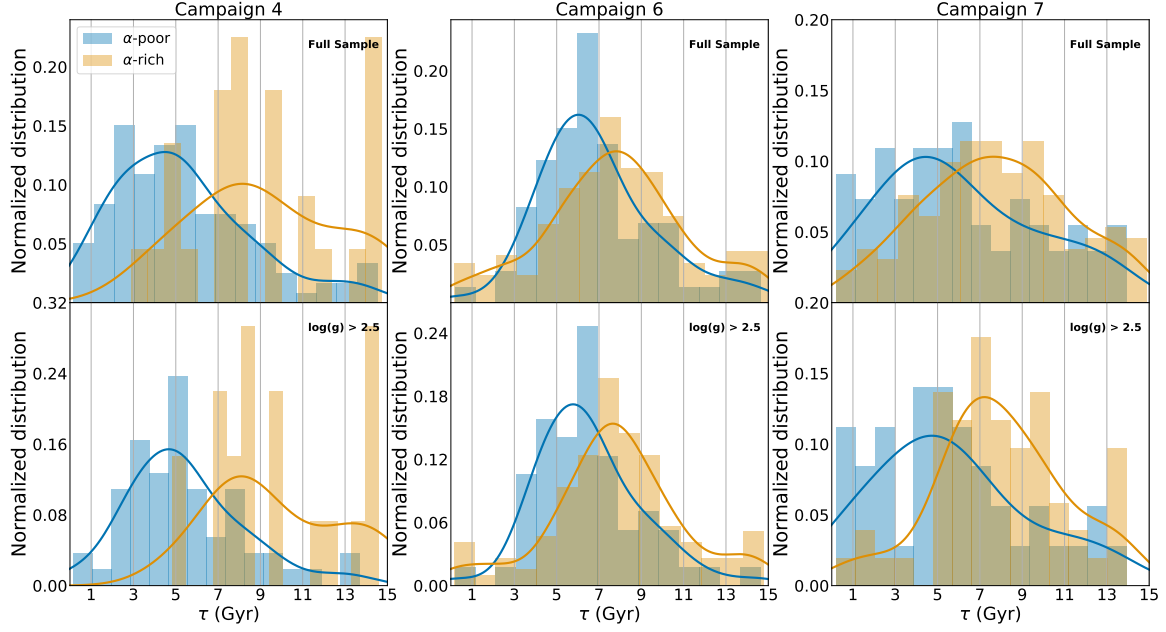


Figure 6. Distributions of the age estimates for both the α -poor (blue) and α -rich (orange) populations for each $K2$ field individually. The top row shows the distributions for the full sample for the respective fields and the bottom row shows the distributions for the low-luminosity sample ($\log(g)_{\text{seis}} > 2.5$). In C4, there are 32 (22) α -rich and 128 (62) α -poor stars in the full (low-luminosity) sample. In C6, there are 335 (208) α -rich and 76 (59) α -poor stars in the full (low-luminosity) sample. In C7, there are 167 (61) α -rich and 66 (39) α -poor stars in the full (low-luminosity) sample.

Table 3. The partial data table for $K2$ campaigns 4, 6, and 7, including our ages. The complete table is available in machine-readable format in the online journal, which also includes the asteroseismic values from each of the individual pipelines.

K2 EPIC ID	K2 Campaign	APOGEE ID	τ (Gyr)	$\sigma^-(\tau)$	$\sigma^+(\tau)$	RA (deg.)	Dec (deg.)	<i>Gaia</i> Designation			
210495151.0	4	2M03593912+1519463	9.94	1.81	2.28	59.913042	15.329524	Gaia DR2 40120290241918848			
210610252.0	4	2M04211626+1706358	9.48	1.71	2.48	65.317758	17.109962	Gaia DR2 3313915749626906752			
210483090.0	4	2M03585776+1507226	2.98	0.36	0.38	59.740697	15.122972	Gaia DR2 40110463356775296			
210505442.0	4	2M04003325+1530162	4.41	1.17	1.65	60.138593	15.504482	Gaia DR2 40147159557282560			
210720697.0	4	2M04220023+1839546	3.62	0.66	0.88	65.500938	18.665140	Gaia DR2 47563498628339072			

T_{eff} (K)	$\sigma(T_{\text{eff}})$	$\log(g)$ (cgs)	$\sigma(\log(g))$	$[\alpha/\text{M}]$	$\sigma([\alpha/\text{M}])$	$[\text{Fe}/\text{H}]$	$\sigma([\text{Fe}/\text{H}])$	$\bar{\nu}_{\text{max}}$ (μHz)	$\sigma(\bar{\nu}_{\text{max}})$	$\Delta\bar{\nu}$ (μHz)
4797.24	106.18	2.87	0.07	0.23	0.01	-0.58	0.01	108.47	0.82	10.36
4750.61	85.03	2.61	0.06	0.04	0.01	-0.23	0.01	44.15	0.60	5.19
4958.78	89.15	3.15	0.06	0.04	0.01	-0.01	0.01	183.08	1.38	14.02
4889.04	91.34	2.84	0.07	0.06	0.01	-0.48	0.01	68.83	0.68	7.10
4726.70	83.11	2.58	0.06	0.01	0.01	-0.09	0.01	52.67	0.59	5.50

$\sigma(\Delta\bar{\nu})$	$\log(g)_{\text{seis}}$ (cgs)	$\sigma(\log(g)_{\text{seis}})$	M (M_{\odot})	$\sigma(M)$	d (kpc)	$\sigma(d)$	X (kpc)	Y (kpc)	Z (kpc)	R (kpc)
0.10	2.94	0.01	0.96	0.05	1.11	0.05	-9.28	0.07	-0.48	9.28
0.04	2.55	0.01	1.01	0.06	1.24	0.08	-9.44	0.04	-0.45	9.44
0.02	3.18	0.01	1.45	0.05	2.35	2.66	-10.37	0.15	-1.07	10.38
0.14	2.75	0.01	1.19	0.11	1.14	0.05	-9.31	0.07	-0.49	9.31
0.05	2.63	0.01	1.35	0.08	1.58	0.12	-9.77	0.08	-0.55	9.77

Table 4. The partial data table for RGB stars in the *Kepler* field. The complete table is available in machine-readable format in the online journal.

KIC	APOGEE ID	τ (Gyr)	$\sigma^-(\tau)$	$\sigma^+(\tau)$	APOKASC2 τ (Gyr)	T_{eff} (K)	$\sigma(T_{\text{eff}})$	$\log(g)$ (cgs)	$\sigma(\log(g))$	$[\alpha/M]$	$\sigma([\alpha/M])$
1027337	2M19252021+3647118	5.49	1.09	1.27	6.28	4635.50	78.02	2.76	0.05	0.01	0.01
1296068	2M19264481+3658152	10.31	1.34	1.68	10.42	4586.52	93.37	2.61	0.05	0.05	0.01
1429505	2M19225688+3702125	6.42	0.96	1.20	7.36	4682.15	87.07	2.64	0.06	0.02	0.01
1431059	2M19243068+3701290	7.71	1.22	1.68	6.98	4802.11	106.14	3.07	0.06	0.00	0.01
1433730	2M19265020+3703054	1.35	0.16	0.21	1.43	4732.06	83.20	2.53	0.06	0.00	0.01

[Fe/H]	$\sigma([\text{Fe}/\text{H}])$	ν_{max} (μHz)	$\sigma(\nu_{\text{max}})$	$\Delta\nu$ (μHz)	$\sigma(\Delta\nu)$	M (M_{\odot})	$\sigma(M)$	X (kpc)	Y (kpc)	Z (kpc)	R (kpc)
0.20	0.01	73.97	0.67	7.09	0.09	1.29	0.08	-7.81	1.31	0.26	7.92
-0.02	0.01	59.38	0.53	6.32	0.02	1.04	0.04	-7.72	1.57	0.31	7.88
-0.11	0.01	55.41	0.61	5.91	0.02	1.15	0.05	-7.88	1.13	0.24	7.96
0.06	0.01	170.84	1.54	13.86	0.08	1.14	0.05	-7.83	1.26	0.26	7.93
-0.08	0.01	40.01	0.36	4.17	0.02	1.79	0.07	-7.91	1.06	0.22	7.98

that an intermediate aged α -rich population is not unthinkable. At the moment, the comparison of our results to Anders et al. 2017’s can only be qualitative. As opposed to SA18, Pinsonneault et al. (2018), Zinn et al. (2020), and this work, Anders et al. (2017) does not apply theoretically-motivated $\Delta\nu$ corrections to their asteroseismic results, which could result in an offset of around 30% in age.

It should be noted that, though there is significantly more spread in the ages around the α -rich peak in the *K2* fields, there is no evidence that this spread is due to anything other than the larger uncertainties associated with this data.

It is also interesting to note that the ages of these two populations seem to converge as a function of height above the Galactic plane, a trend that is shown in Figure 7. Hayden et al. (2017) finds similar trends, such that coeval populations of α -rich and α -poor stars are found to have the same vertical scale heights. These results potentially coincide with those from Rendle et al. (2019), whose *K2* Galactic archaeology results seem consistent with the “upside-down” formation model (e.g., Bird et al. 2013), wherein stars form in a vertically-extended disk, with subsequent formation occurring closer and closer to the Galactic plane.

We also tentatively recover the young, α -rich stars seen in the *Kepler* analysis of SA18 and the *K2* analysis of Rendle et al. (2019). The origin of these stars has not been definitively determined, but part of the population may be explained by stellar mergers.

To analyse the meaning of these results, it may be useful to place them within the context of the proposed scenarios in the literature for generating the bi-modal α sequence, each of which comes with their own set of predictions concerning the relative ages of α -rich and

α -poor populations and the homogeneity of these ages throughout the Galaxy.

One of these possible mechanisms is the radial migration of stars mixing together populations of different chemical origins. In this scenario, the radial migration of stars born at different radii in the disk results in the superposition of several chemical evolution sequences at any given location in the Galaxy. Stars with high $[\alpha/\text{Fe}]$ at high $[\text{Fe}/\text{H}]$, for example, could come from inner regions where more efficient star formation produced high metallicity gas relatively quickly. When mixed together, they form the sequence that we are familiar with. Therefore, the primary explanation for the lack of an age-metallicity relation is mostly attributed to stellar neighbors not having necessarily been born from the same gas, as stars have moved radially inwards and outwards in their orbits (see e.g. Schönrich & Binney 2009; Weinberg et al. 2017; Nidever et al. 2014; Sharma et al. 2020). However, it is not entirely clear whether our results of similar α -rich populations having strongly peaked ages in different parts of the Galaxy is consistent with this theory.

Another possible explanation is that the two loci of the bi-modal α sequence are the products of two gas infall episodes that both spurred two independent periods of star formation. In this scenario, the α -rich sequence was formed during a rapid infall episode that occurred about 10 billion years ago. This would be followed by a drought of star formation that would itself be followed by a gradual infall episode spurring star formation from about 8 billion years ago to present. The pristine gas in this second infall would dilute the disk gas, creating a new starting point at lower $[\text{Fe}/\text{H}]$ for a second, less α -enriched episode (Chiappini et al. 1997). Each of these star formation episodes would revive historic

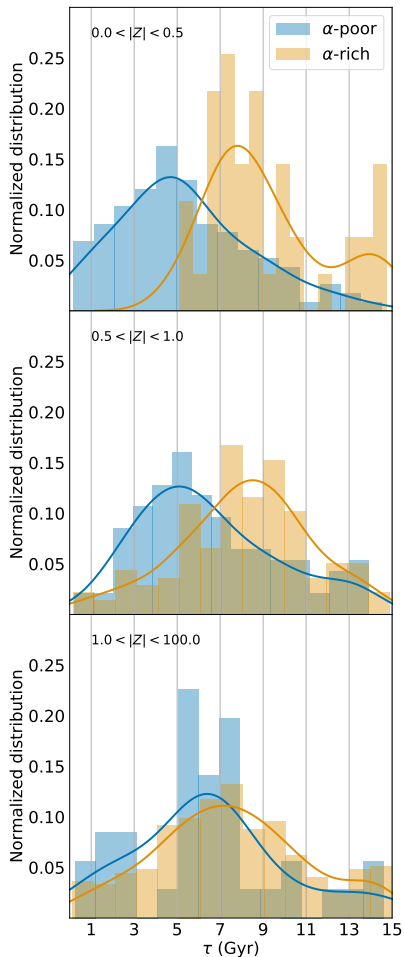


Figure 7. Distributions of the age estimates for both the α -poor and α -rich of the *K2* fields as a function of distance from the Galactic plane $|Z|$. While the median age of the α -rich population is about constant as a function of vertical height, if not slightly decreasing with $|Z|$, the α -poor population seems to increase in age as $|Z|$ increases, with the populations converging on an age of about 7 Gyr.

rates of SNe II, but have lesser effects on changing the rate of SNe Ia. Spitoni et al. (2019), simulating this two-infall scenario, were able to successfully replicate the bi-modal α sequence as well as the age trends found in SA18 for the high- and low- α sequences. Lian et al. (2020) present a similar model which is able to better produce the density ridge-line between the α -rich and α -poor loci while also being able to more accurately reproduce the observed ages of α -poor stars. Adding the *K2* data, however, seems to suggest that this two-infall scenario would have to be at least slightly more complex if star formation happened at different times in different places in the Galaxy during the first, rapid episode. Sharma et al. (2020) points out that the model by Spitoni et al. (2019) requires a loop in the tracks in the

$[\alpha/\text{Fe}]$ vs. $[\text{Fe}/\text{H}]$ plane which does not agree with observations. Figure 8 shows the *K2* sample in the $[\alpha/\text{Fe}]$ vs. $[\text{Fe}/\text{H}]$ plane with stars colored by their ages, but it is not clear that our results have the resolution nor the volume needed to fully explore the existence of this age loop.

A third proposed mechanism is that the bi-modal sequence is the product of star formation happening in clumpy bursts throughout the Galaxy. In this scenario, there is a background of star formation within the α -poor sequence and the rest of the star formation takes place in gas-rich clumps that naturally arose in the disk. When star formation is spurred in these clumps, these populations of stars are initially enriched with α elements as the number of SNe II is spurred by the formation of new, massive stars. Therefore, in this scenario, the α -rich sequence is formed from a superposition of these clumpy star formation episodes (see e.g. Clarke et al. 2019). If assuming that the populations are not mixed together (by, for example, radial migration), this allows nearly identical chemical populations observed in different regions of the Galaxy to have diverging ages. This mechanism therefore seems promising as a potential explanation for why similar chemical populations in different parts of the Galaxy would have strongly peaked, discrepant ages. However, since the ages of the α -rich populations in the three *K2* fields seem to agree with each other but disagree the age of the α -rich population in the *Kepler* field, if this scenario is true, it is still curious why only the very local Galaxy seems to be unique in its star formation history.

Looking forward, the third data release of the *K2* Galactic Archaeology Program will provide us with asteroseismic data for giants along fourteen more lines of sight in the Galaxy. Additionally, a similar analysis is possible with data from NASA’s ongoing Transiting Exoplanet Survey Satellite mission. This data, along with the spectroscopy from the final APOGEE data releases and from other large-scale surveys, can be used to fill in a more complete picture of the age gradients for stellar populations throughout the Milky Way.

ACKNOWLEDGMENTS

This paper is dedicated to the memory of Nikki Justice.

Funding for the Sloan Digital Sky Survey IV has been provided by the Alfred P. Sloan Foundation, the U.S. Department of Energy Office of Science, and the Participating Institutions. SDSS-IV acknowledges support and resources from the Center for High-Performance Com-

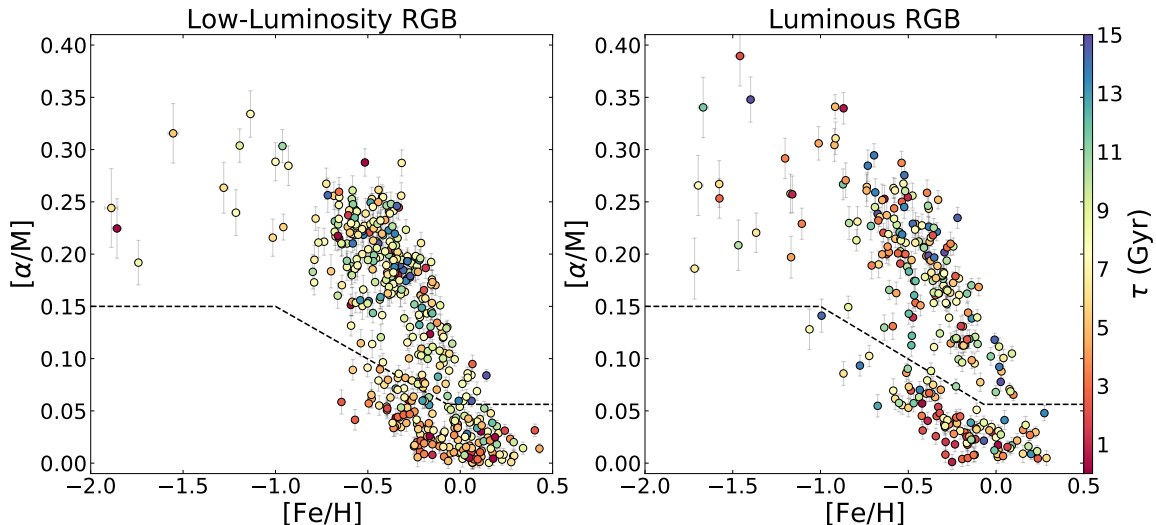


Figure 8. $[\alpha/M]$ vs. $[Fe/H]$ for the low-luminosity and luminous giants in our sample, colored by age.

puting at the University of Utah. The SDSS web site is www.sdss.org.

SDSS-IV is managed by the Astrophysical Research Consortium for the Participating Institutions of the SDSS Collaboration including the Brazilian Participation Group, the Carnegie Institution for Science, Carnegie Mellon University, the Chilean Participation Group, the French Participation Group, Harvard-Smithsonian Center for Astrophysics, Instituto de Astrofísica de Canarias, The Johns Hopkins University, Kavli Institute for the Physics and Mathematics of the Universe (IPMU) / University of Tokyo, the Korean Participation Group, Lawrence Berkeley National Laboratory, Leibniz Institut für Astrophysik Potsdam (AIP), Max-Planck-Institut für Astronomie (MPIA Heidelberg), Max-Planck-Institut für Astrophysik (MPA Garching), Max-Planck-Institut für Extraterrestrische Physik (MPE), National Astronomical Observatories of China, New Mexico State University, New York Uni-

versity, University of Notre Dame, Observatório Nacional / MCTI, The Ohio State University, Pennsylvania State University, Shanghai Astronomical Observatory, United Kingdom Participation Group, Universidad Nacional Autónoma de México, University of Arizona, University of Colorado Boulder, University of Oxford, University of Portsmouth, University of Utah, University of Virginia, University of Washington, University of Wisconsin, Vanderbilt University, and Yale University.

JTW and MHP acknowledge support from NASA Grant 80NSSC19K0115. RAG acknowledges the support of the PLATO CNES grant. SM would like to acknowledge support from the Spanish Ministry through the Ramon y Cajal fellowship number RYC-2015-17697. DAGH acknowledges support from the State Research Agency (AEI) of the Spanish Ministry of Science, Innovation and Universities (MCIU) and the European Regional Development Fund (FEDER) under grant AYA2017-88254-P.

REFERENCES

- Ahumada, R., Prieto, C. A., Almeida, A., et al. 2020, *ApJS*, 249, 3
- Aller, L. H., & Greenstein, J. L. 1960, *ApJS*, 5, 139
- Anders, F., Chiappini, C., Rodrigues, T. S., et al. 2017, *A&A*, 597, A30
- Astropy Collaboration, Robitaille, T. P., Tollerud, E. J., et al. 2013, *A&A*, 558, A33
- Bailer-Jones, C. A. L. 2015, *PASP*, 127, 994
- Bedding, T. R., Mosser, B., Huber, D., et al. 2011, *Nature*, 471, 608
- Bensby, T., Feltzing, S., & Lundström, I. 2003, *A&A*, 410, 527
- Bird, J. C., Kazantzidis, S., Weinberg, D. H., et al. 2013, *ApJ*, 773, 43
- Blanton, M. R., Bershady, M. A., Abolfathi, B., et al. 2017, *AJ*, 154, 28
- Bovy, J., Nidever, D. L., Rix, H.-W., et al. 2014, *ApJ*, 790, 127
- Bowen, I. S., & Vaughan, A. H. 1973, *Appl. Opt.*, 12, 1430
- Brown, T. M., Gilliland, R. L., Noyes, R. W., & Ramsey, L. W. 1991, *ApJ*, 368, 599
- Casagrande, L., Silva Aguirre, V., Schlesinger, K. J., et al. 2016, *MNRAS*, 455, 987

- Chaplin, W. J., Houdek, G., Appourchaux, T., et al. 2008, *A&A*, 485, 813
- Chiappini, C., Matteucci, F., & Gratton, R. 1997, *ApJ*, 477, 765
- Chiappini, C., Anders, F., Rodrigues, T. S., et al. 2015, *A&A*, 576, L12
- Clarke, A. J., Debattista, V. P., Nidever, D. L., et al. 2019, *MNRAS*, 484, 3476
- da Silva, L., Girardi, L., Pasquini, L., et al. 2006, *A&A*, 458, 609
- Elsworth, Y., Themeßl, N., Hekker, S., & Chaplin, W. 2020, *Research Notes of the American Astronomical Society*, 4, 177
- Elsworth, Y., Hekker, S., Johnson, J. A., et al. 2019, *MNRAS*, 489, 4641
- Epstein, C. R., Elsworth, Y. P., Johnson, J. A., et al. 2014, *ApJL*, 785, L28
- Fuhrmann, K. 1998, *A&A*, 338, 161
- . 2011, *MNRAS*, 414, 2893
- Gaia Collaboration, Prusti, T., de Bruijne, J. H. J., et al. 2016, *A&A*, 595, A1
- Gaia Collaboration, Brown, A. G. A., Vallenari, A., et al. 2018, *A&A*, 616, A1
- García Pérez, A. E., Allende Prieto, C., Holtzman, J. A., et al. 2016, *AJ*, 151, 144
- Gilmore, G., & Reid, N. 1983, *MNRAS*, 202, 1025
- Guggenberger, E., Hekker, S., Angelou, G. C., Basu, S., & Bellinger, E. P. 2017, *MNRAS*, 470, 2069
- Gunn, J. E., Siegmund, W. A., Mannery, E. J., et al. 2006, *AJ*, 131, 2332
- Hayden, M. R., Recio-Blanco, A., de Laverny, P., Mikolaitis, S., & Worley, C. C. 2017, *A&A*, 608, L1
- Hayden, M. R., Bovy, J., Holtzman, J. A., et al. 2015, *ApJ*, 808, 132
- Hekker, S., Broomhall, A. M., Chaplin, W. J., et al. 2010, *MNRAS*, 402, 2049
- Holtzman, J. A., Hasselquist, S., Shetrone, M., et al. 2018, *AJ*, 156, 125
- Howell, S. B., Sobek, C., Haas, M., et al. 2014, *PASP*, 126, 398
- Huber, D., Stello, D., Bedding, T. R., et al. 2009, *Communications in Asteroseismology*, 160, 74
- Huber, D., Zinn, J., Bojsen-Hansen, M., et al. 2017, *ApJ*, 844, 102
- Jönsson, H., Holtzman, J. A., Allende Prieto, C., et al. 2020, *AJ*, 160, 120
- Kallinger, T., Hekker, S., Garcia, R. A., Huber, D., & Matthews, J. M. 2016, *Science Advances*, 2, 1500654
- Khan, S., Miglio, A., Mosser, B., et al. 2019, *A&A*, 628, A35
- Kjeldsen, H., & Bedding, T. R. 1995, *A&A*, 293, 87
- Lian, J., Thomas, D., Maraston, C., et al. 2020, *MNRAS*, 494, 2561
- Majewski, S. R., Schiavon, R. P., Frinchaboy, P. M., et al. 2017, *AJ*, 154, 94
- Mamajek, E. E., Prsa, A., Torres, G., et al. 2015, *arXiv e-prints*
- Martig, M., Rix, H.-W., Silva Aguirre, V., et al. 2015, *MNRAS*, 451, 2230
- Mathur, S., García, R. A., Régulo, C., et al. 2010, *A&A*, 511, A46
- Miglio, A., Chiappini, C., Mackereth, T., et al. 2020, *arXiv e-prints*
- Montalbán, J., Mackereth, J. T., Miglio, A., et al. 2020, *arXiv e-prints*, [arXiv:2006.01783](https://arxiv.org/abs/2006.01783)
- Mosser, B., & Appourchaux, T. 2009, *A&A*, 508, 877
- Mosser, B., Dziembowski, W. A., Belkacem, K., et al. 2013, *A&A*, 559, A137
- Nidever, D. L., Bovy, J., Bird, J. C., et al. 2014, *ApJ*, 796, 38
- Nidever, D. L., Holtzman, J. A., Allende Prieto, C., et al. 2015, *AJ*, 150, 173
- Pinsonneault, M. H., Kawaler, S. D., Sofia, S., & Demarque, P. 1989, *ApJ*, 338, 424
- Pinsonneault, M. H., Elsworth, Y., Epstein, C., et al. 2014, *ApJS*, 215, 19
- Pinsonneault, M. H., Elsworth, Y. P., Tayar, J., et al. 2018, *ApJS*, 239, 32
- Price-Whelan, A. M., Sipőcz, B. M., Günther, H. M., et al. 2018, *AJ*, 156, 123
- Prochaska, J. X., Naumov, S. O., Carney, B. W., McWilliam, A., & Wolfe, A. M. 2000, *AJ*, 120, 2513
- Rendle, B. M., Miglio, A., Chiappini, C., et al. 2019, *MNRAS*, 490, 4465
- Rodrigues, T. S., Girardi, L., Miglio, A., et al. 2014, *MNRAS*, 445, 2758
- Salaris, M., Chieffi, A., & Straniero, O. 1993, *ApJ*, 414, 580
- Schönrich, R., & Binney, J. 2009, *MNRAS*, 396, 203
- Sellwood, J. A., & Binney, J. J. 2002, *MNRAS*, 336, 785
- Sharma, S., Hayden, M. R., & Bland-Hawthorn, J. 2020, *arXiv e-prints*, [arXiv:2005.03646](https://arxiv.org/abs/2005.03646)
- Sharma, S., Stello, D., Bland-Hawthorn, J., Huber, D., & Bedding, T. R. 2016, *ApJ*, 822, 15
- Silva Aguirre, V., Davies, G. R., Basu, S., et al. 2015, *MNRAS*, 452, 2127
- Silva Aguirre, V., Lund, M. N., Antia, H. M., et al. 2017, *ApJ*, 835, 173
- Silva Aguirre, V., Bojsen-Hansen, M., Slumstrup, D., et al. 2018, *MNRAS*, 475, 5487
- Spitoni, E., Silva Aguirre, V., Matteucci, F., Calura, F., & Grisoni, V. 2019, *A&A*, 623, A60

- Stello, D., Huber, D., Sharma, S., et al. 2015, *ApJL*, 809, L3
- Stello, D., Zinn, J., Elsworth, Y., et al. 2017, *ApJ*, 835, 83
- Tayar, J., Somers, G., Pinsonneault, M. H., et al. 2017, *ApJ*, 840, 17
- Tinsley, B. M. 1979, *ApJ*, 229, 1046
- Ulrich, R. K. 1986, *ApJL*, 306, L37
- Valentini, M., Chiappini, C., Bossini, D., et al. 2019, *A&A*, 627, A173
- van Saders, J. L., & Pinsonneault, M. H. 2012, *ApJ*, 746, 16
- Wallerstein, G. 1962, *ApJS*, 6, 407
- Waskom, M., Botvinnik, O., O’Kane, D., et al. 2017, *mwaskom/seaborn*: v0.8.1 (September 2017), v0.8.1, Zenodo
- Weinberg, D. H., Andrews, B. H., & Freudenburg, J. 2017, *ApJ*, 837, 183
- Weinberg, D. H., Holtzman, J. A., Hesselquist, S., et al. 2019, *ApJ*, 874, 102
- White, T. R., Bedding, T. R., Stello, D., et al. 2011, *The Astrophysical Journal*, 743, 161
- Wilson, J. C., Hearty, F. R., Skrutskie, M. F., et al. 2019, *PASP*, 131, 055001
- Zasowski, G., Johnson, J. A., Frinchaboy, P. M., et al. 2013, *AJ*, 146, 81
- Zasowski, G., Cohen, R. E., Chojnowski, S. D., et al. 2017, *AJ*, 154, 198
- Zinn, J. C., Pinsonneault, M. H., Huber, D., et al. 2019a, *ApJ*, 885, 166
- Zinn, J. C., Stello, D., Huber, D., & Sharma, S. 2019b, *ApJ*, 884, 107
- Zinn, J. C., Stello, D., Elsworth, Y., et al. 2020, *ApJS*, 251, 23